Electrochemical Sensor for Ascorbic Acid, Acetaminophen and Nitrite Based on Organoclay/Zr-MOF Film Modified Glassy Carbon Electrode

Marcelline Carine Ngo Ngwem[a], Prof. Justin Claude Kemmegne-Mbouguen[a*], Prof. Henrietta W. Langmi[b*], Dr. Nicholas M. Musyoka[c] and Prof. Robert Mokaya[d]

[a]Laboratory of Nanomaterials for Sensors and Energy, Faculty of Science, University of Yaounde I, P.O.Box. 812 Yaounde, Cameroon

[b]Department of Chemistry, University of Pretoria, Private Bag X20, Hatfield 0028, South Africa

[c]Nanostructures and Advanced Materials (CeNAM), Chemicals Cluster, Council for Scientific and Industrial Research (CSIR), Meiring Naude Road, Brummeria, Pretoria, 0001, South Africa

[d]School of Chemistry, University Park, University of Nottingham, Nottingham NG7 2RD, United Kingdom

***To whom correspondence should be addressed:**

e-mail: jkemmeg@yahoo.fr, phone: + 237 666 091225 and

e-mail: henrietta.langmi@up.ac.za; phone: +27 (0)12 420 2800

Abstract

A composite (Sa-HTDMA/UiO-66) consisting of organoclay (Sa-HTDMA) and a metal-organic framework (UiO-66) was prepared using organically modified natural Cameroonian clay and Zr-MOF. The organoclay was obtained by intercalating in its interlayer hexadecyltrimethyl ammonium cation (HTDMA). The composite was then used to form a film onto a glassy carbon electrode (GCE) by drop coating (Sa-HTDMA/UiO-66/GCE). Electrochemical responses recorded at the as-prepared modified electrodes for ascorbic acid (AA), acetaminophen (AC) and nitrite (NO_2^-) were investigated using cyclic and linear sweep voltammetry. The results revealed that Sa-HTDMA/UiO-66/GCE exhibited a favorable behavior for individual and simultaneous sensing of AA, AC and NO_2^-. Additionally, compared with UiO-66 modified GCE, the composite enabled good performance of the electrode. Under the optimum conditions, the linear calibration curves were attained in the following ranges: 1-650 µM for AA, 1-700 µM for AC and 1-600 µM for NO_2^- with the respective detection limits of 0.01, 0.19 and 0.33µM. Application of the sensors to determine AA and AC in pharmaceutical preparations, and NO_2^- in tap water, was successful.

Introduction

Ascorbic acid (AA) also referred to as vitamin C is an antioxidant that is present in the human diet. While it is an essential vitamin, excessive intake of AA can lead to digestive distress, headache, insomnia, and flushing of the skin [1]. An important electrochemical characteristic of AA is its electroactivity at both platinum and carbon electrodes and hence electrochemistry is an interesting method for its detection. However, the oxidation of AA requires undesirably high overvoltage. This overvoltage is usually associated with poor selectivity and sensitivity, poor reducibility, and fouling of the electrode [2]. Acetaminophen (N-acethyl-p-aminophenol also referred to as paracetamol, AC) is one of most used drugs as an antipyretic and analgesic compound. When administered in the correct therapeutic dose, AC does not show detrimental side effects such as those associated with the liver and kidney [3]. AC may also be employed to achieve selective and sensitive fluorimetric detection of nitrite (NO_2^-) [4].

Nitrite plays a vital role in food, environmental, and physiological systems [5]. In physiological processes, it can be produced from oxidation of nitric oxide, known as a messenger within the cardiovascular system [6]. In aqueous solution without biological material, NO_2^- is the result of autooxidation of oxide [7]. Its presence in excess amounts in blood will lead to ferrohemoglobin oxidation [8]. In addition, NO_2^- is used as a corrosion inhibitor in some foods [9]. Thus, the quantification of NO_2^- has increasing interest [6]. In this framework, several methods including spectroscopy, chromatography and spectrofluorimetry have been used for this purpose. Although these techniques were successful, electrochemical sensors have appeared to be promising for the determination of NO_2^- due to a fast response, facile operation and low cost [10]. However, as for AA, the determination of NO_2^- ion on the bare solid electrode is restricted as the electrode surface tends to be poisoned by some species generated in the course of the electrochemical process, which reduces its sensitivity and accuracy [11]. A good way to overcome this limitation is by the modification of the electrode surface with an appropriate

stable film. Therefore, different chemically modified electrodes have been explored for the oxidation of NO_2^- [10, 12]. Because AA, AC, and NO_2^- coexist in physiological fluids and are electroactive, it is important to determine their concentration using electrochemical sensors with more sensitivity and selectivity.

Metal-organic frameworks (MOFs) are a category of hybrid porous crystalline materials composed of metal ions linked with organic ligands. They have diverse and interesting properties including permanent porosity, tunable pore size, crystalline structure and high surface area. Thanks to these properties, MOFs have been used for various applications such as gas storage [13], catalysis [14] and as sensors [15]. In spite of the interesting properties of MOFs, their ability to form stable films on solid electrodes and their aggregation in aqueous medium have long been considered as major obstacles to their application in electrochemistry. To overcome these issues, many researchers have explored combining MOFs with other materials resulting in composites in order to prepare more stable electrochemical based MOF sensors with good selectivity and sensitivity. Recently, Wang and co-workers reported a dopamine electrochemical sensor based on glassy carbon modified with a film of a composite made of Al-MIL-53 and nafion [16]. Likewise, Zhou and co-workers demonstrated the synthesis of a Cu-MOF-199 and single–walled carbon nanotube composite that exhibited some desirable features for electrode modification for selective determination of cathecol and hydroquinone [17]. In other work, Qial and co-workers used reduced graphene to prepare a sensor based on graphene foam and UiO-66 [18]. Recently, we have reported an electrochemical quantification of two analytes, AC and tryptophan, simultaneously at a Zr-MOF/graphene foam film modified glassy carbon [19]. Although MOF-based composites show satisfactory results, to date the materials typically combined with MOFs are expensive, not always accessible and difficult to handle. In addition, it is important to move away from the use of expensive substrates as starting materials so as to realize the green synthesis of MOF composites using natural and environmentally

friendly matter such as minerals. In this regard, clay minerals, which are naturally available, non-polluting, easy to access and less expensive, could enable the synthesis of MOF-clay composites with desirable properties.

Clay minerals are among the most abundant materials on earth. They are aluminosilicates of nanoscale dimension with interesting properties such as ion exchange ability, thermal and mechanical stability, and swelling and porosity properties. Thanks to their capability of capturing and releasing organic molecules, clays have been applied in various fields particularly in food, agriculture and environmental remediation [20]. Interestingly, the possibility to modify, by chemisorption and physisorption, the surface and the interlayer of clay [21], provides the opportunity to generate new materials with enhanced properties and applications relative to pristine clay. Thus, because of the unique properties, i.e. a combination of ion exchange, swelling and intercalation, it is possible to intercalate cationic organic ions into clay. Furthermore, such modified clays have good affinity for organic molecules [22]. Since the introduction of the use of clay in electrochemistry by Gosh and Bard in 1983 [23], clay and organoclay modified electrode have been successfully exploited as electrochemical sensors [24], biosensors [25] and immunosensors [26].

Taking advantage of the above characteristics of organoclay and MOF, we have used hexadecyltrimethyl ammonium bromide-functionalized clay (Sa-HDTMA) and Zr-MOF (UiO-66) composite to fabricate a sensing interface in order to attain the detection of AA, AC and NO_2^- simultaneously in aqueous media. The sensor displayed attractive response performances arising from the derived synergistic effect of the two component materials of the composite.

Results and Discussion

Physicochemical characterisation of organoclay and organoclay/MOF composite

*Physicochemical characterisation of the organoclay (*Sa-HTDMA)

Sa-Na^+ was expanded by ion exchange of $HDTMA^+$ cation, and powder X-ray diffraction (XRD) was used to probe the displacement of the clay sheets by observing the shift of the (001) diffraction peak to a lower 2θ angle. Fig 1A shows the XRD patterns of pristine clay before (curve a) and after the loading of $HDTMA^+$ cation (curve b). The basal spacing values for the clay (Sa-Na^+) and Sa-HTDMA, which correspond to the peaks at the lowest 2θ values, were found to be 12.6 Å and 17 Å, respectively. These results imply that the basal spacing of treated clay is expanded as a result of the intercalation of $HDTMA^+$ and the degree of expansion was estimated to be ca. 6.4 Å. This value indicates that the organic cation intercalated into clay with a plane of its carbon atoms in a zigzag manner parallel to the plane of the clay sheets, given that the size of $HDTMA^+$ is roughly 4.2 Å (height) by 23.5 Å (width) [27].

The Fourier Transform-Infrared (FT–IR) spectra of Sa-Na^+ (curve a) and Sa-HTDMA (curve b) are presented in Fig. 1B. In curve a, a very small band ascribed to the –OH stretching vibration of the unmodified clay, was observed at ca. 3626 cm^{-1}. Curve a also exhibits broad bands at *ca*. 3463 cm^{-1} and 1630 cm^{-1}, which correspond to the bending modes of vibration of adsorbed water within the pristine clay. In addition, the band at 1053 cm^{-1} is ascribed to the asymmetric stretching vibration mode of the Si–O–Si backbone of the clay. A siloxane band is observed at 1053 cm^{-1} in the pristine clay (curve a). This band shifts to 1037 cm^{-1} in Sa-HTDMA (curve b) emphasizing the importance of siloxane groups in cationic surfactant adsorption onto clay [28]. Bands occurring at 2926 cm^{-1} and 2854 cm^{-1} for the organoclay (curve b) are attributed to C–H stretching vibrations. Interestingly, these bands are not observed for the pristine clay,

implying the successful intercalation of the surfactant into the organoclay. The results likely indicate that $HDTMA^+$ existed in the interlayer space of the clay, and that the surface of the clay was altered from being hydrophilic to hydrophobic [22].

***Physicochemical characterisation of the composite organoclay/ZrMOF (*Sa-HTDMA/UiO-66)**

The XRD pattern of UiO-66 (Fig. 1A, curve d) exhibited peaks at 2θ values of 7.397°, 8.534°, 12.062°, 17.076°, 22.230° and 25.747° corresponding to the (111), (002), (022), (004), (115) and (006) crystal planes, respectively. This is consistent with previous reports [13, 29], and confirms that UiO-66 was synthesized successfully. It can also be noticed that UiO-66/Sa-HTDMA composites (Fig. 1A, curve c) displayed the characteristic diffraction peaks of UiO-66 and the organoclay, implying that the composite was successfully formed whilst UiO-66 remained intact. It is well known that smectite clays are composed of layers or compacted plates, thus changes in clay morphology are expected due to addition of nanoparticulated UiO-66. The expected behavior on dispersion of nanoparticulated Zr MOF onto clay is a partial coating of clay aggregates, according to the dry dispersion procedure [30]. Consequently, the clay agglomerates serve as a base for the dispersion of the Zr-MOF as shown in Fig. 2B.

The FT-IR spectrum of pristine UiO-66 (Fig. 1B, curve d) shows the characteristic stretching vibrations of UiO-66. Bands at 1578 and 1396 cm^{-1} correspond, respectively, to the asymmetric and symmetric stretches of the carboxylate. Meanwhile, the bands observed at 657 and 546 cm^{-1} are attributed to Zr–O stretching and Zr-(OC) asymmetric stretching vibrations, respectively. Comparing the Sa-HTDMA/UiO-66 composite's spectrum (Fig. 1B curve c) with that of the pristine MOF, one can observe that the position of the vibration bands did not change, which suggests that the presence of organoclay did not alter the UiO-66.

Electrochemical characterisation of the organoclay/ZrMOF film electrode (Sa-HTDMA/UiO-66/GCE)

A preliminary investigation to assess the ability of Sa-HTDMA/UiO-66 composite to form a thin and stable film on GCE was carried out using the composite film electrode, Sa-HTDMA/UiO-66/GCE. It was conducted by evaluating the electrochemical behavior of an anionic probe ($Fe(CN)_6^{3-}$) at UiO-66 and Sa-HTDMA/UiO-66 modified glassy carbon, by obtaining a series of cyclic voltammograms (CVs) in diluted $Fe(CN)_6^{3-}$. The Multisweep voltammograms recorded at bare GCE, UiO-66/GCE and Sa-HTDMA/UiO-66/GCE are shown in Fig. 3. At bare GCE (Fig. 3A) and UiO-66/GCE (Fig. 3B), distinct diffusion controlled redox behavior with a constant steady state current was obtained upon scanning repeatedly at 50 $mV.s^{-1}$. The CVs obtained at UiO-66 modified electrode were centered at E°' (equal *to 1/2*(E_{pred} + E_{pox})) = +0.234 V with peak-to-peak separation ΔE (equal to E_{pox} - E_{pred}) value of 0.183 V. Even though the steady currents obtained with bare GCE were slightly higher than those at UiO-66 modified glassy carbon, the peak-to-peak separation obtained using bare GCE was found to decrease by 20 mV relative to that obtained at modified electrode. Interestingly, when the UiO-66 film was made with less concentrated MOF suspension, ΔE_p obtained with UiO-66 /GCE decreased to *ca*. 22 mV with a slight increase in peak current (Figure S1) when compared to that recorded at bare GCE. These results suggest that when MOF film is thicker, it likely constitutes a barrier vis-a-vis the redox anionic probe, and thus its diffusion is more difficult at Zr-MOF modified GCE. When composite modified electrodes (Sa-HTDMA/UiO-66/GCE) were used, well defined redox behavior was also obtained and repetitive potential scans led to a continuous increase of the electrochemical signals which attained their maximum (7.5 μA) after 40 cyclic scans and thereafter stayed almost unchanged. At Sa-HTDMA/UiO-66/GCE, the CVs obtained were centered at E°' = + 0.112 V, with ΔE = 0.065 V. This peak-to-peak value was ~ 62 mV lower relative to that obtained when using UiO-66/GCE. This result implies that

the diffusion of the probe is easier at Sa-HTDMA/UiO-66/GCE. This behavior can be explained by the presence of the positively charged organic cation within the clay, which has ensued from ion exchange and hydrophobic bonding. Thus, the conversion of pristine clay from a negatively to a positively charged organoclay has favored the electrostatic interaction between the anionic probe and organoclay, and consequently the Sa-HTDMA/UiO-66 film, thus inducing anionic probe uptake through the formation of surface-anion complex [31].

To evaluate the surface area of the modified and bare electrode, the Randles-Sevcik equation below (Eq. 1) was applied and $K_3[FeCN_6]$ used as probe (Fig. S2 A and C).

$$Ip=2.69\ x\ 10^5\ x\ (D_o)^{1/2}Av^{1/2}n^{3/2}Co \quad (1)$$

Here, for $[Fe(CN)_6]^{3-/4-}$, n =1, Co = 5 x 10^{-7} mol.cm^{-3}, Do = 1 x 10^{-5} cm^2 s^{-1}[32], consequently, the surface area of Sa-HTDMA/UiO-66/GCE was found to be 0.083 cm^2. This value is 3.6 times that of surface of pristine UiO-66 film electrode and 2.4 times that of bare GC electrode. This result proved that the organoclay likely improved the dispersion of the nanosized MOF in the composite and enhanced the surface area of GCE. The substantial increase in the electroactive surface area of the composite film modified electrode demonstrated that Sa-HTDMA/UiO-66/GCE is promising for electrochemical sensing.

Electrochemical properties of Sa-HTDMA/UiO-66/GCE in the presence of AA, AC and NO_2^-

Linear sweep voltammogram (LSV) and CV were used to highlight the electrocatalytic properties of Sa-HTDMA/UiO-66 film modified GCE (Sa-HTDMA/UiO-66/GCE) toward AA, AC and NO_2^-. Figure 4A compares LSVs recorded at bare GCE (curve a), UiO-66/GCE (curve b) and Sa-HTDMA/UiO-66/GCE (curve c) in 0.01 M acetate buffer (AB) pH 5 containing 620 µM of AA, 671 µM of AC, and 620 µM of NO_2^-. The composite modified GCE gave rise to three distinct oxidation peaks attributed to the electrochemical oxidation of AA (at +0.369 V),

AC (at +0.585 V) and NO_2^- (at +0.918 V). Interestingly, when bare GCE was used in the same conditions, these oxidation peaks also appeared on the LSV, but their peak potentials were found to shift positively by about 78 mV for AA, 90 mV for AC and 194 mV for NO_2^-. As can be seen on curve b (Fig. 4A) obtained at UiO-66/GCE in the electrolyte solution that contained three analytes, two distinct oxidation peaks occurred at +0.627 V and +1.064 V belonging to the electrooxidation of AC and NO_2^-, respectively, with a small hump at + 0.362 V as a result of AA oxidation. In fact, when the electrolyte pH is 5, AA (pKa1 = 4.17) [33] is negatively charged , hence, the poor sensitivity observed at Zr-MOF modified electrode can be explained on the basis of electrostatic interactions between AA and the UiO-66 surface: the oxidation of AA is difficult on the negatively charged UiO-66 film owing to electrostatic repulsion. From these results, it can be observed that the modification of GCE with a composite film significantly enhanced the electrocatalytic activity of Sa-HTDMA/UiO-66/GCE in comparison with bare GCE and UiO-66/GCE. The outstanding performance of Sa-HTDMA/UiO-66/GCE might be attributed to the fact that adding positively charged organoclay could have avoided the collapse of the MOF and reinforced its structure during measurement, and favored electrostatic interaction with negatively charged NO_2^- and AA. Then this will likely facilitate the reaction between hydroxyl group of the analytes and Zr(IV).

Figure 4B displays the CVs recorded using Sa-HTDMA/UiO-66/GCE in the same conditions as above in the presence of the analyte mixture within the potential window at a scan rate of 5 mVs^{-1}. The cyclic voltammograms of AA, AC and NO_2^- recorded at Sa-HTDMA/UiO-66/GCE when potential was scanned in the positive direction displayed well-defined oxidation peaks. On the reverse scan with the same scan rate, except for AC, no cathodic peak was seen within the studied potential range for AA and NO_2^-, since their oxidation is known to be an electrochemical irreversible process [34]. Two quasi-reversible redox peaks were evident for AC with peak potential centred at +0.455 V.

The presence of the organoclay as part of the composite affects the electrooxidation of the three analytes at Sa-HTDMA/UiO-66/GCE. The dependence of the LSV oxidation peak current of AA, AC and NO_2^- on various amounts of organoclay in the composite film modified electrode is provided in Fig. S3. Starting from a film of Zr-MOF free of organoclay, the oxidation peaks of AC and NO_2^- appeared well-defined whereas that of AA was not. Interestingly, increase in the amount of organoclay led to the appearance of three well-defined oxidation peaks ascribed to the oxidation of the three analytes, reaching a maximum value when the film was made with the composite composed of 70 % of MOF and 30 % of organoclay. This increase of the electrochemical response between 0 – 30 % of organoclay is likely because of increased adsorption sites from organoclay and its positive charge. Above 30% of organoclay content, the responses due to analyte oxidation decrease as the amount of organoclay in the composite increases. This observation may be due to the fact that the presence of a large amount of non-conductive organoclay has induced a decrease of electrode conductivity. A mass ratio of Sa-HTDMA/UiO-66 of 30/70 was therefore used in further investigation.

Figure 5A exhibits the effect of the scan rate (5-50 $mV.s^{-1}$) on the electrochemical response of the oxidation of AA, AC and NO_2^-. For all three analytes, the oxidation and cathodic (for AC only) current obtained were proportional to the square root of the scan rate within the scan range explored. This result indicates that for the three analytes in the investigated scan rate range, the redox reactions at Sa-HTDMA/UiO-66/GCE are diffusion-controlled processes.

It is well known that when the slope of the plot of log of peak current against log of scan rate equals 0.5, the electrochemical reaction involved is diffusion-controlled and when it is 1, this reaction is controlled by adsorption. The log of peak current versus log of scan rate for the three analytes was plotted (Fig. 5B).The plots of log of peak current ($\log I_p$) vs. log scan rate ($\log \nu$) for 620 µM AA (curve a), 671 µM AC (curve b') and 620 µM NO_2^-(curve c) were linear ($R^2 = 0.995$) with 0.36, 0.40 and 0.42 as slope values, respectively. The obtained slopes are

close to 0.5, which suggests that the electrooxidation of the three analytes was controlled principally by diffusion at Sa-HTDMA/UiO-66/GCE and the analytes did not foul the surface of the electrode.

To determine some important parameters involved in the electrochemical reaction of the analytes at Sa-HTDMA/UiO-66/GCE, such as the number of electrons (n) in the rate controlling step and the transfer coefficient (α), the Laviron theory [35] was used. In this regard, for the three analytes, the peak potential versus the log of scan rate was plotted and evaluated. For AA, AC and NO_2^-, the peak potentials E_{pa} and/or E_{pc} showed a linear dependence on log *v* (as seen in Fig. 5C) with the following regression equations (Eqs. 2 to 5):

For AC (curve b' and b for oxidation and reduction process, respectively):

E_{pa} =0.50 + 0.039 log *v* (R^2 = 0.977)…… …… …… (2)

E_{pc}= 0.49 – 0.082 log *v* (R^2 = 0.995) (3)

For AA (curve a):

E_{pa} = 0.29 + 0.055log *v* (R^2 = 0.962) (4)

And for NO_2^- (curve c):

E_{pa} = 0.84 + 0.052 log *v* (R^2 = 0.978) (5)

At UiO-66/GCE, the peak potentials were linearly dependent on log *v* for AC and NO_2^- (Fig. S4). The peak potential corresponding to AA oxidation was not suitable for exploitation. Thus for AC (Eqs. 6 and 7),

E_{pa} =0.574 + 0.032 log *v* (R^2 = 0.953)…… …… (6)

E_{pc}= 1.013 – 0.043 log *v* (R^2 = 0.977) (7)

For NO_2^- (Eq. 8):

E_{pa} = 0.29 + 0.053 log *v* (R^2 = 0.974) (8)

For a reversible process, E_p is linearly dependent on log *v* and gives a pair of straight lines having slopes of $2.3\ RT/(1-\alpha)nF$ and $-2.3\ RT/\alpha nF$ for the oxidation and reduction peaks,

respectively, according to Laviron theory; R, T and F being respectively, the gas constant, temperature and Faraday constant. Using the slopes from Eq. 2 and 3 of both straight lines (exhibited as curves b' and b in Fig 5C), the charge transfer coefficient obtained was 0.32 and the number of electrons transferred in this electrochemical redox reaction was 2.2 ≈ 2 at Sa-HTDMA/UiO-66/GCE. This number of electrons transferred is the same as previously reported for organoclay modified electrode toward AC [21b, 36]. Interestingly, from the slopes of Eq. 6 and 7 (seen Fig. S4), the transfer coefficient was found to be 0.43, indicating that the number of electrons involved in the electrochemical oxidation of AC was 3.2 at UiO-66/GCE. This number was 1.6 times greater than the 2 electrons expected for the oxidation of AC, suggesting that the oxidation of AC at UiO-66/GCE likely interfered with that of AA at this electrode.

A Tafel plot was exploited to determine the number of electrons participating in the completely irreversible diffusion controlled process of AA and NO_2^-, following the equation (Eq. 9) [35]:

$$Epa = K + \left(\frac{b}{2}\right) log v \qquad (9)$$

Where b is the Tafel slope and *v* the scan rate. For AA, the plot of E_p versus log *v* (Eq. 4 and 5) as shown in Fig. 5C, led to a slope value of 0.055 (curve a). Thus at Sa-HTDMA/UiO-66/GCE, for the oxidation of AA, b = 2 x 55 i.e., 110 mV. This slope indicates that at Sa-HTDMA/UiO-66/GCE for AA, the rate determining step involved a one electron process assuming a transfer coefficient α = 0.5. A Tafel plot was also drawn using data obtained from the current voltage curve of CV recorded at 5 $mV.s^{-1}$ (Fig. S5) to confirm the information about the rate-determining step. Thus, from the polarization measurement, a slope of 102 $mV.decade^{-1}$ is obtained and close to that of b obtained from $\partial Ep/\partial(\log v)$ from Eq. 9 . This result indicates a one electron transfer to be the rate limiting step with α = 0.58 The corresponding mechanism of the oxidation of AA is presented in scheme 1 (A). Given that at pH 5, the AA is deprotonated, the proposed mechanism involved the obtained monoionic species of AA forming a radical ion

which then underwent a one electron oxidation to give dehydroascorbic acid [37]. For NO_2^- ion, at UiO-66/GCE, the Tafel slope was found to be 2*0.053 i.e. 0.106 V very close to b = 2 x 0.052 obtained at HTDMA/UiO-66/GCE, suggesting that, as expected, the NO_2^- oxidation at both modified electrodes involved one electron assuming the transfer coefficient α = 0.5. This result also indicated that at HTDMA/UiO-66/GCE, the oxidation of AA and AC did not interfere with that of NO_2^-. The mechanisms of the electrochemical reaction of NO_2^- and AC are shown in scheme 1B and 1C, respectively.

The apparent heterogeneous electron transfer rate constant denoted k_s at HTDMA/UiO-66/GCE was calculated using Eq. 10 for reversible process and Eq. 11 for irreversible process [35].

$$\log k_s = \alpha \log (1-\alpha) + (1-\alpha) \log \alpha - \log (RT/nFv) - \alpha(1-\alpha)nF\Delta E_P/2.3RT \quad (10)$$

$$E_p = E_o + (2.303RT/\alpha nF) \log (RTk_S/\alpha nF) + (2.303RT/\alpha nF) \log v \quad (11)$$

From the above equation, the k_ss value was calculated to be 1.4 s^{-1}, 0.39 s^{-1} and 1.23 s^{-1} for AA, AC and NO_2^-, respectively.

In order to study the involvement of protons in the redox behavior of the target electroactive analytes, the effect of the pH of the support electrolyte on the redox process was examined. The LSVs recorded in the electrolytic solution at different pH containing 620 µM AA, 671 µMAC and 620 µM NO_2^- are shown in Fig. 6. It was observed that when the pH decreased, the anodic peak potential shifted positively, indicating that H^+ participated in the electrochemical process at Sa-HTDMA/UiO-66/GCE involving AA and AC. For these two analytes, the oxidation peak potentials shifted linearly versus pH, obeying the regression equation: E_p= 0.52 – 0.04 pH (R^2 = 0.994) for AA and E_p= 0.75 – 0.04 pH (R^2 = 0.993) for AC. The slopes obtained for AA and AC from the regression equation were close to the 59 mV/pH (25 °C) theoretical value which suggests the transfer of the same number of protons and electrons during electrochemical process. Interestingly, for NO_2^- oxidation, the peak potential was nearly constant in the operating pH ranges, implying that its oxidation was not affected by

the pH of electrolyte support. This is consistent with previous reports on NO_2^-oxidation [10, 12, 38]. This behavior can be ascribed to a kinetically governed oxidation reaction *i.e.* a catalytic step that is independent of protons [12, 38]. It was also observed that the electrochemical response of the oxidation of the three analytes was influenced by the pH of the electrolyte support. For AA and AC, the oxidation peak currents were found to increase when pH increased from 3.5 to 5, and subsequently declined for pH values exceeding 5. While for NO_2^-, the electrochemical response was not significantly affected by the pH of the electrolyte solution. The latter behavior was also reported in the literature. Considering the favourable oxidation peak current of AA, AC and NO_2^-, AB pH 5 was used for the individual and simultaneous detection.

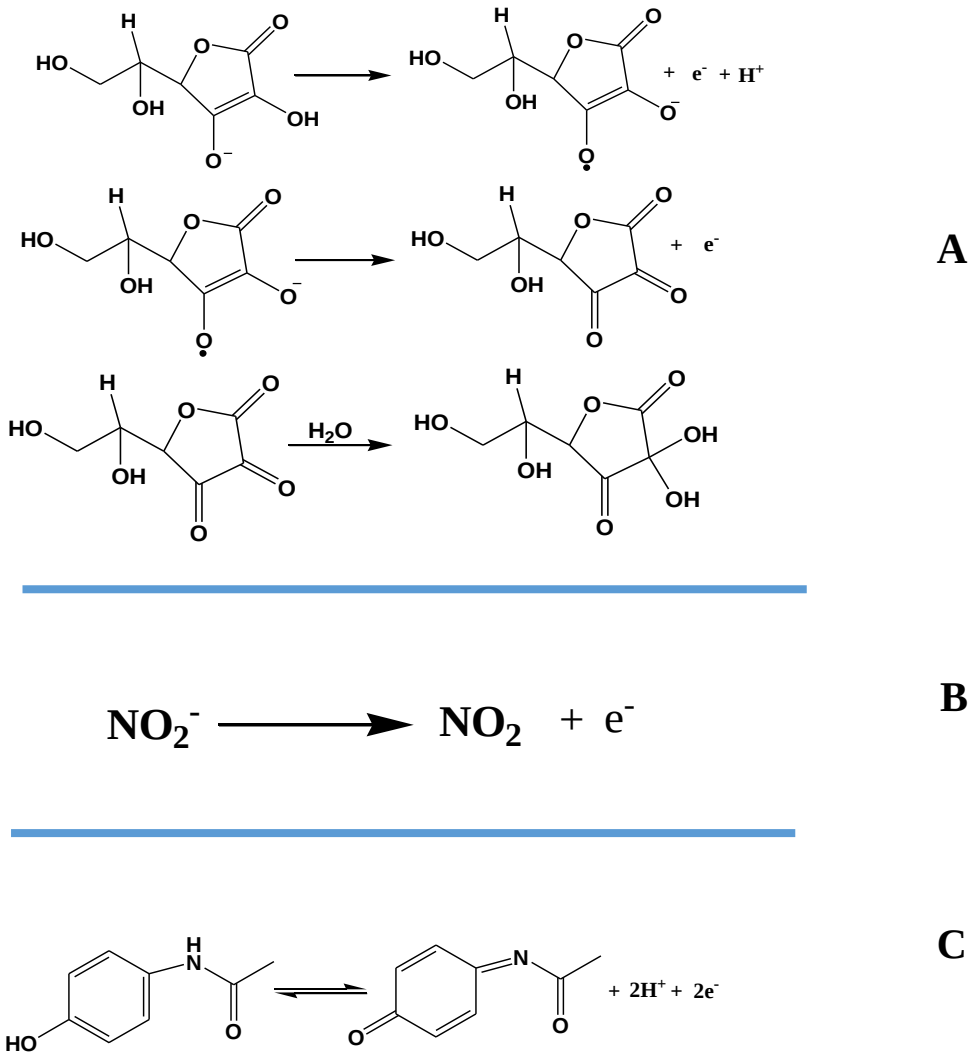

Scheme 1: The mechanisms of the electrochemical reaction of (A) AA, (B) NO_2^- and (C) AC at Sa-*HTDMA/UiO-66/GCE*

Individual and simultaneous determination of AA, AC and NO_2^- at Sa-HTDMA/UiO-66/GCE

Figure 7 shows the LSV response recorded at +0.369 V for AA (Fig. 7A), at +0.585 V for AC (Fig. 7B), and at +0.918 V for NO_2^- (Fig. 7C) using Sa-HTDMA/UiO-66/GCE when increasing amount of each analyte was solely added in AB pH 5. The peak current in each case corresponds to a constant increase of individual analyte concentration. As can be seen in the insets of Fig. 7, the electrochemical response depends linearly on the concentration of each

analyte within the concentration ranges 1 – 650 µM (R^2=0.989), 1 – 700 µM (R^2=0.995) and 1 – 600 µM (R^2=0.997) with the limits of detection being 0.01 µM, 0.19 µM and 0.33µM (S/N = 3), respectively. Furthermore, the sensitivity of Sa-HTDMA/UiO-66/GCE was estimated to be 0.0182 µA/µM, 0.0181 µA/µM and 0.0094 µA/µM for AA, AC and NO_2^-, respectively.

Using the same experimental conditions, the simultaneous determination of AA, AC and NO_2^- at Sa-HTDMA/UiO-66/GCE was investigated. Figure 8 shows the LSV curves recorded at Sa-HTDMA/UiO-66/GCE at various concentrations of AA, AC and NO_2^-. When the electrolyte solution contained these three analytes, three discrete anodic peaks were evident with a significant difference between oxidation peak potentials. The oxidation peak potential for each analyte is in agreement with that obtained when the oxidation of each analyte was studied individually, which confirms that the concurrent determination of AA, AC and NO_2^- is favored when in a mixture. Upon increasing the concentration of the three analytes simultaneously, the peak current due to the oxidation of these analytes increased as shown by the LSVs of Fig. 8A. The inset of this figure 8A indicates that the electrochemical responses recorded at Sa-HTDMA/UiO-66/GCE for each analyte AA, AC and NO_2^- were linearly dependent on their concentration (with R^2 = 0.995) with the sensitivity of 0.016 µA/µM for AA, 0.0158 µA/µM for AC, and 0.010 µA/µM for NO_2^-. These sensitivities are consistent with those obtained at Sa-HTDMA/UiO-66/GCE when the electrolyte contained only one analyte. Remarkably, as shown in Fig. 8B, when an increased amount of NO_2^- was added in AB solution (pH = 5) with a constant concentration of AA (620 µM) and AC (671 µM), the peak current associated with the electrooxidation of NO_2^- increased while those due to the oxidation of AA and AC remained largely constant. As can be seen from Fig. 8C, this behavior is also exhibited when an increased amount of AC was added in an electrolyte solution that contained AA (620 µM). These results demonstrate that there was no interference between the three biological species studied. From each calibration curve, the sensitivity of Sa-HTDMA/UiO-66/GCE was

estimated to be 0.019 µA/µM for AC and 0.11 µM for NO_2^-. The performance of the fabricated sensor, including the detection limit and linear range, are presented in table 1 alongside some values found in the literature. It is clear that the proposed sensor from the current study demonstrated limits of detection that are superior or at least comparable to those reported by other studies.

Interference study

Using the optimized conditions; the effect of possible interfering species on the simultaneous detection of AA, AC and NO_2^- (10 µM) was investigated in AB (pH 5). It was found that 15-fold saccharin, citric acid, glucose, sodium carbonate, (less than 1 mM) did not have any obvious interference with the current electrochemical response of AA, AC and NO_2^-. Uric acid and dopamine were found to interfere with AA determination. The influence of other possible inorganic (10 Mm of Ca^{2+}, Mg^{2+} or Zn^{2+}) interferences on the sensors response toward these analytes was also investigated and were observed not to cause any limitations to the determination of the analytes (signal changed below 5%).

Reproducibility and stability of the modified electrode Sa-HTDMA/UiO-66/GCE

In an effort to check the reproducibility of electrode, five prepared modified glassy carbon electrodes (Sa-HTDMA/UiO-66/GCE) were tested under optimum conditions. The relative standard deviation was 6.2 %, 3.0 % and 5.1 % for AA, AC and NO_2^-, respectively. This result confirms that the electrode modification using composite suspension had a high reproducibility. Furthermore, the long-term stability of the as-prepared sensor Sa-HTDMA/UiO-66/GCE (stored in AB (pH 5) at room temperature when not in use) was investigated using a calibration plot for AC in the concentration ranges as mentioned above for

individual detection for about 3 days each. This revealed that the developed sensor maintained ca. 85 % of its initial sensitivity after 15 days (see Fig. S6).

Real samples analysis

Two real pharmaceutical samples: ascorbic acid 1000 (i.e., 1000 mg of ascorbic acid/tablet, with the commercial name Vitamin C) and Paracetamol 500 (i.e., 500 mg of acetaminophen / tablet, trade with the commercial name Paracetamol) were used for evaluation of developed sensor performance. They were both purchased from a local drug store and prepared by dilution with distillated water. They were then analyzed using the standard addition method employing Sa-HTDMA/UiO-66/GCE as the sensor. The LSVs recorded for AA and AC samples are shown in Fig. S6A and S6B, respectively. Experimentally, a tablet of paracetamol or vitamin C was diluted with distillated water in 200 mL volumetric flask. After complete dilution and homogenization, 1 mL of the sample from the prepared solution was then transferred to a 100 mL volumetric flask and the volume toped up with AB (pH 5). From this real solution, 0.5 mL was introduced in the volumetric cell followed by the addition of 9.50 mL of AB (pH 5). The first LSV (dashed line, Fig. S7) was then recorded at Sa-HTDMA/UiO-66/GCE and in sequence five injections (100 µL each) of standard solution was performed and responses recorded (solid line, Fig. S6). The results are presented in Table 2. It is observed that a recovery value of 98% for AA and 92% for AC was attained with respect to the supplier specification. This demonstrates the applicability of the developed sensor.

Experimental recoveries of nitrite in real sample were conducted by addition of known amounts of sodium nitrite to tap water to obtain concentrations of 50, 80 and 150 µM under optimal conditions using Sa-HTDMA/UiO-66/GCE. It can be seen that recovery rates ranging from 98.3 to 107.5 % were achieved (Table S1) by applying the standard addition procedure.

Table 1: Comparison of some modified electrodes for the determination of AA, AC and NO_2^-

Modified electrode	**Linear range (µM)**			**Limit of detection (µM)**			**References**
	AA	**AC**	**NO_2^-**	**AA**	**AC**	**NO_2^-**	
Fe_3O_4@Au/GS-chit/GCE	6-350	0.4-32	-	1.0	0.05	-	[39]
Fc-S-Au/NC/GF/GCE	8-400	0.5-46	-	1.00	0.10	-	[40]
GF/UiO-66/GCE	0.5-200	-	-	0.07	-	-	[19]
GCE/CNO-NiMoO₄ -MnWO₄	1–100	-	-	0.33	-	-	[41]
AgNPs/PVP/GC	2–150	-	-	0.047	-	-	[42]
Au-MOF-5/GCE	-	-	5.0-250			1.0	[43]
PAP-ZrO_2NPs-CNTs/GCE	1-295			0.35			[44]
Au/p-TA/GCE	2.1-50	-	15.9-277	1.1	-	0.89	[45]
CTAB-GO/MWNT/GCE	5-300	-	5-80	1.0	-	1.5	[46]
GF/poly-cyclodextrin/ MWNTs/GCE	5-480	-	5-675	1.65	-	1.65	[47]
Cu^{2+}@*PDA*-MWCNTs	5-175	5-75	4-150	0.82	0.87	0.92	[48]
Sa-HDTMA/UiO-66/GCE	**1-650**	**1-700**	**1-600**	**0.01**	**0.19**	**0.33**	**This work**

Fe_3O_4@Au : ferrocene thiolate stabilized gold nanoparticles, GS-chit *:* graphene sheet/chitosan *Fc-S-Au:*thiol functional ferrocene derivatve (Fc-SH) stabilized goldnanoparticles, *NC:* nanocomposite, *GF :*graphene foam,UiO-66 : zirconium based metal organic framework–,Au: gold particules, MOF-5: zinc based metal organic framework, p-*TA*: poly(3-amino-mercapto-1,2,4 triazole ,CTAB: hexadecyltrimethyl ammonium bromide, GO: graphene oxide , MWNT: multiwalled carbon nanotubes.$Cu^{2+@}$*PDA:* copper polydopaminecomplex, PAP : poly(aminopyrazine), ZrO_2NPs : zirconium oxide nanoparticles, CNTs : carbone nanotubes ; *CNO* : carbon nanoonion ; PVP :Polyvinylpyrrolidone

Table 2: Determination of AA and AC levels in commercial drugs using the Sa-HTDMA/UiO-66/GCE

Pharmaceutical formulation	Label value(mg/tablet)	Found value (mg/tablet)	% recovery
Ascorbic acid	1000	980 ± 3.5	98 %
acetaminophen	500	493± 4.1	91.7%

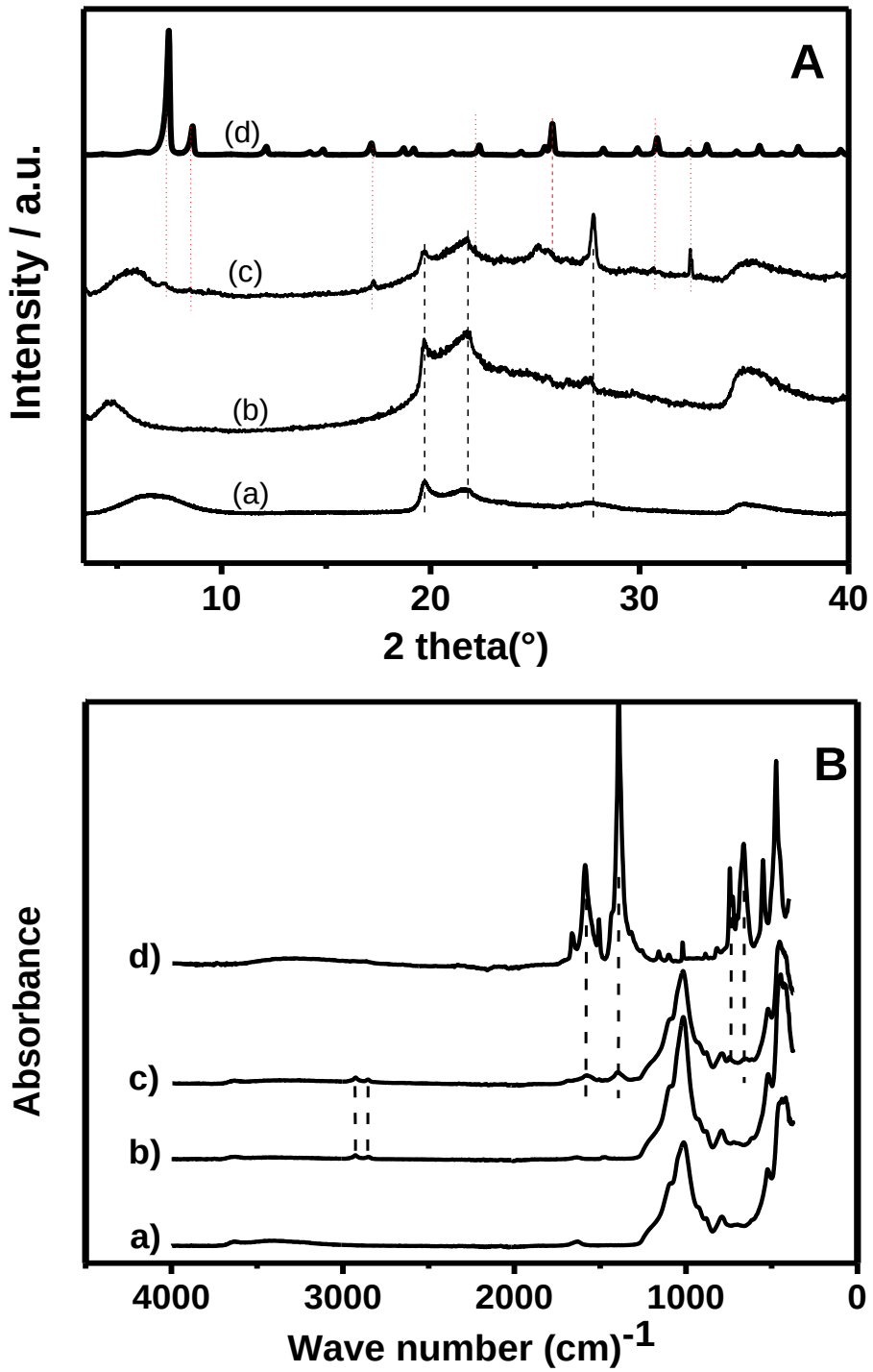

Fig. 1(A) XRD patterns and (B) FT–IR of (a) Sa, (b) Sa-HTDMA, (c) Sa-HTDMA/UiO-66 (d) UiO-66.

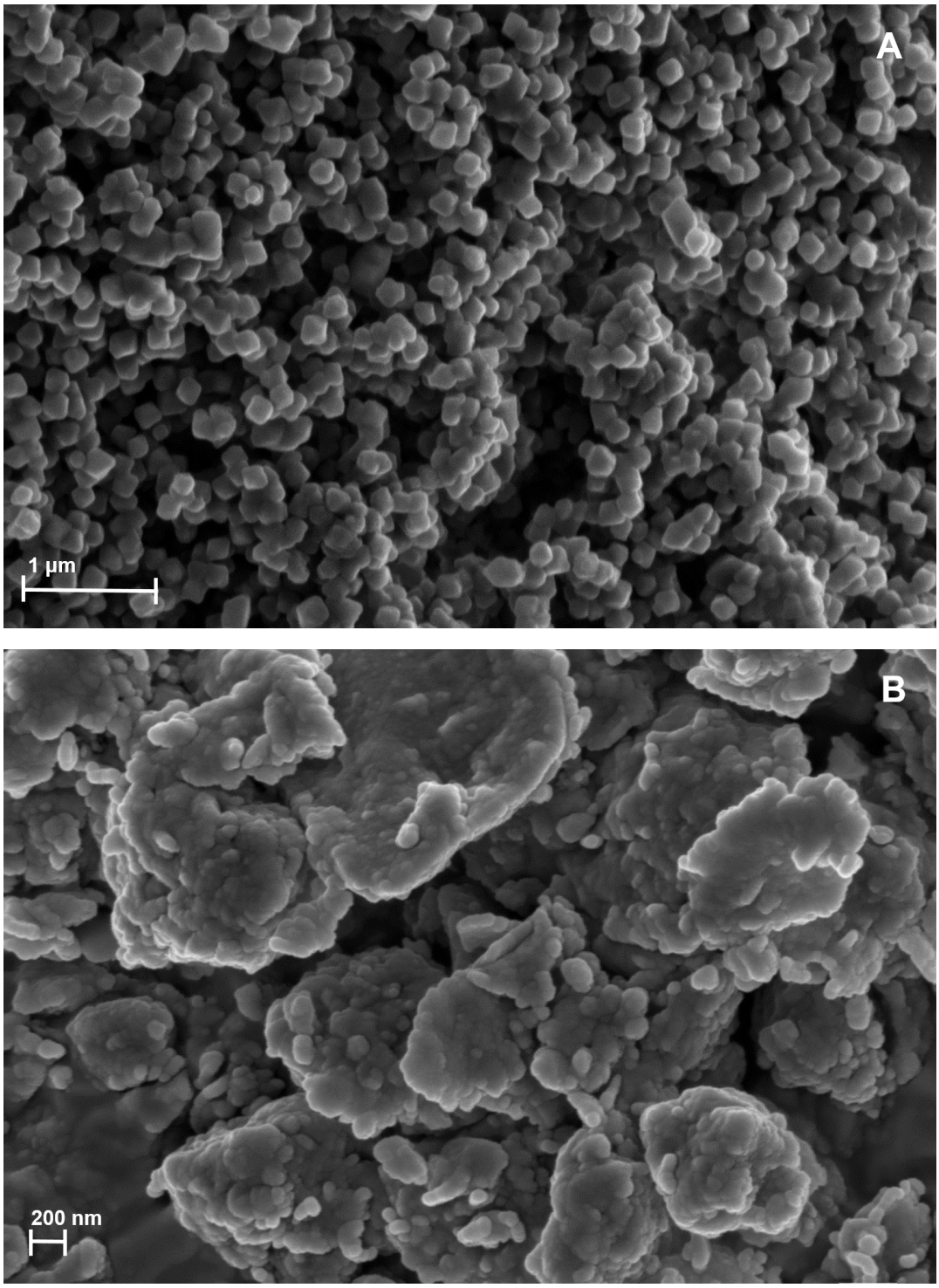

Fig. 2 SEM images of the obtained (A) UiO-66 and (B) Sa-HTDMA/UiO-66

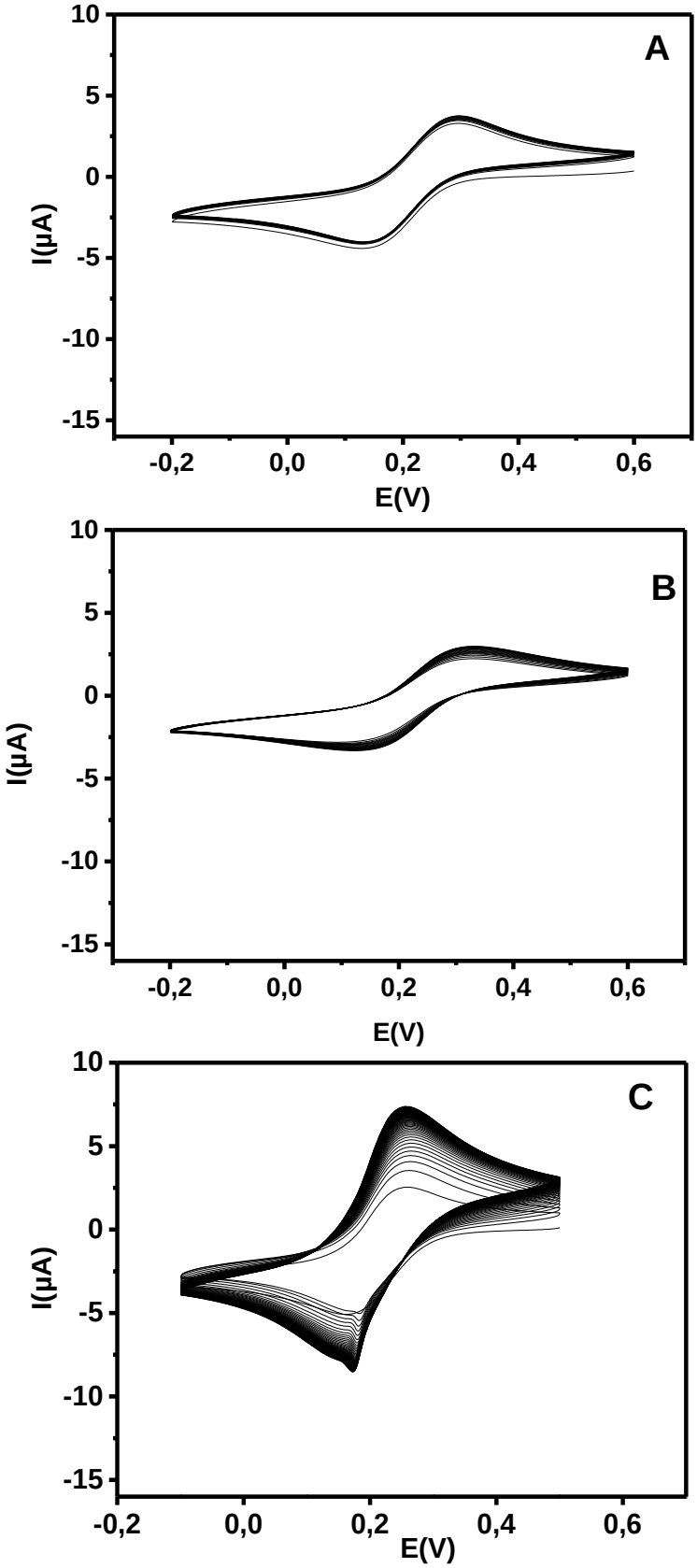

Fig. 3 : Multisweep cyclic voltammograms recorded in 0.1 M KCl containing 0.5 μM $[Fe(CN)6]^{3-}$using (A) bare GCE (B) UiO-66/GCE and (C) Sa-HTDMA/UiO-66/GCE at a scan rate of 50 mV s^{-1}.

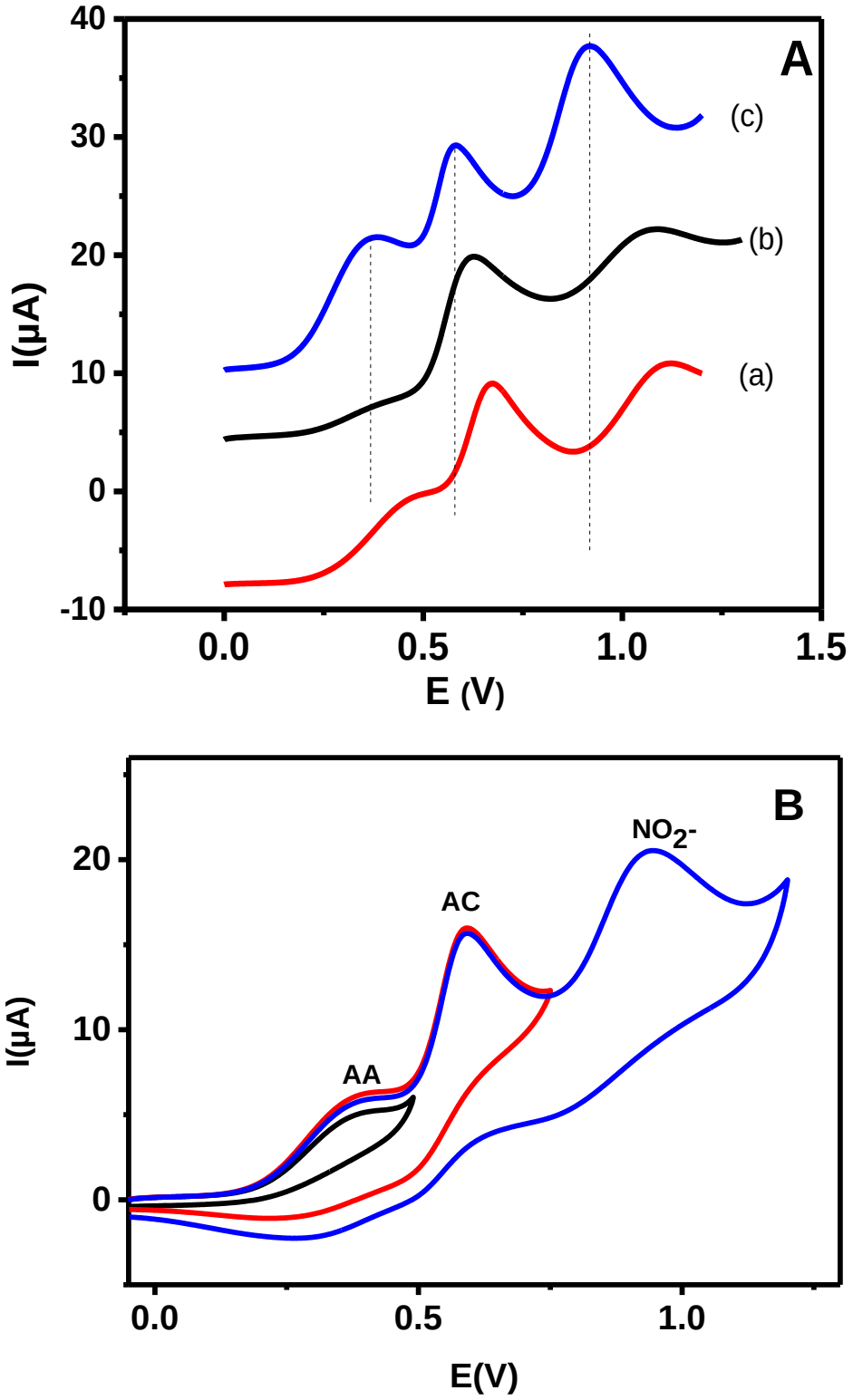

Fig. 4 : (A) LSVs recorded in 0.01 M AB buffer (pH 5) containing 620 µM AA, 671 µM AC and 620 µM NO_2^- at (a) bare GCE, (b) UiO-66/GCE and (c) Sa-HTDMA-UiO-66/GCE. (B) CVs recorded at Sa-HTDMA /UiO-66 /GCE in the same conditions as in (A).

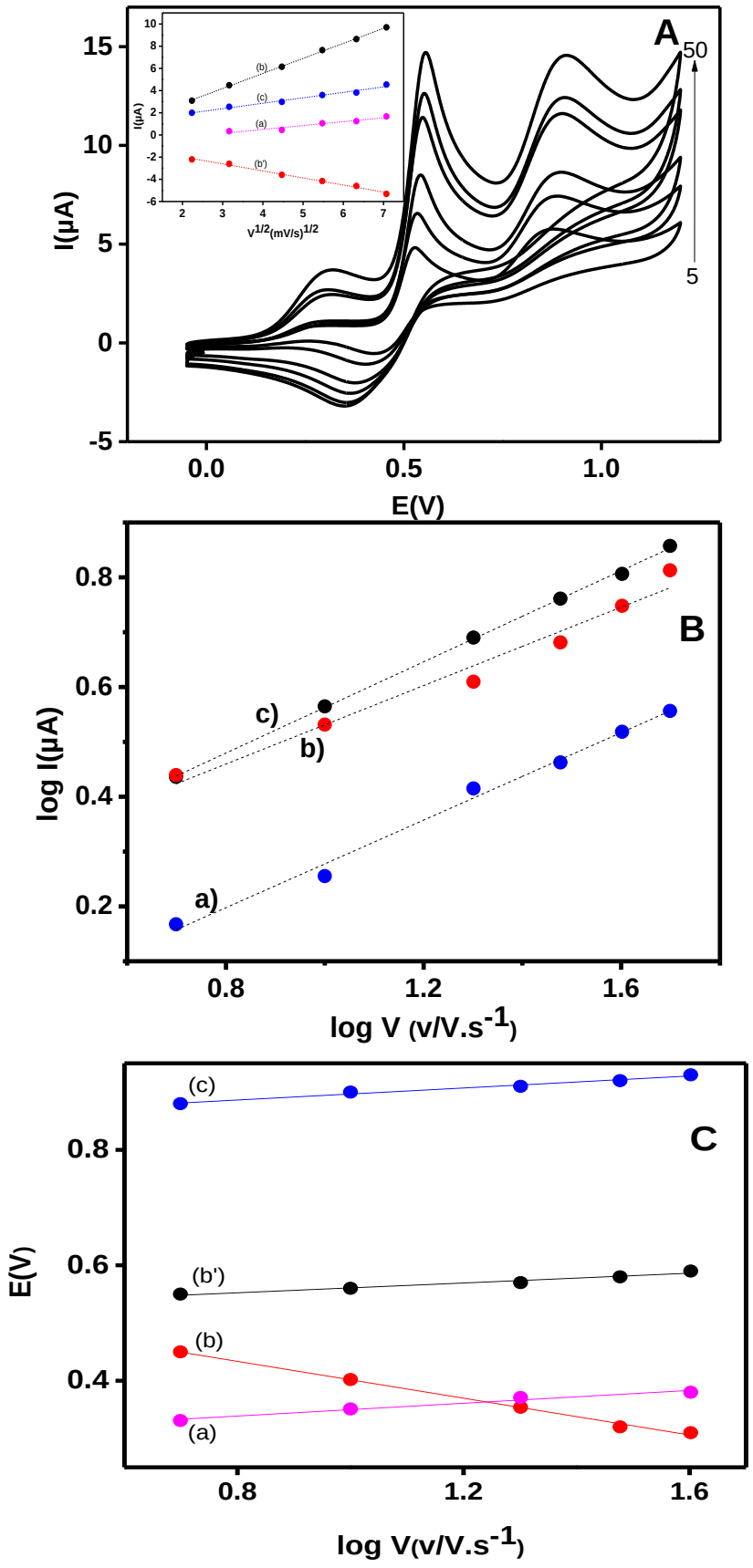

Fig. 5 : (A) Cyclic voltammograms at Sa-HTDMA/UiO-66/GCE in AB (pH 5) containing 620 µM AA, 671 µM AC and 620 µM NO_2^- at different scan rates. Inset show plot of peak currents

of AA (a), AC (b) and NO_2^- (c) vs the square root of scan rate. (B) Plot of log I versus log *v* for (a) AA, (b) AC and (c) NO_2^-. (C) Plot of Ep versus log *v* for (a) AA, (b' and b) AC and (c) NO_2^- .

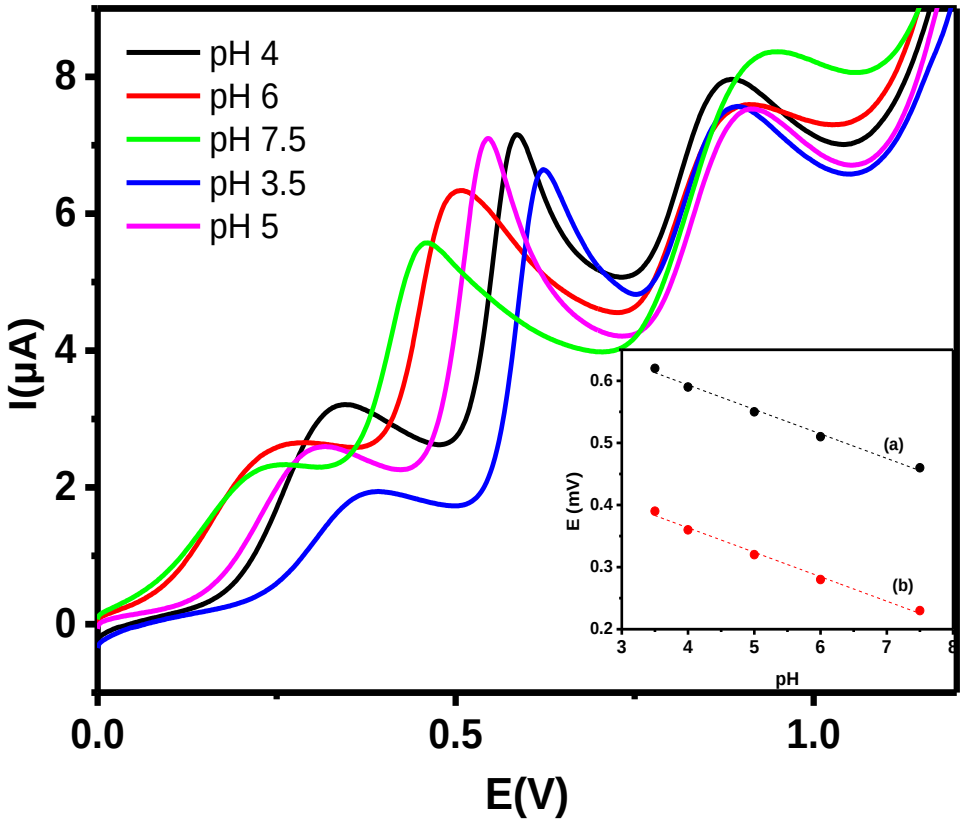

Fig. 6 : LSVs recorded at Sa-HTDMA/UiO-66 in 0.01 M buffer solution at different pH and containing 620 µM AA, 671 µM AC and 620 µM NO_2^-. Inset show plot of the anodic peak currents *vs* pH for AA (a) and AC (b).

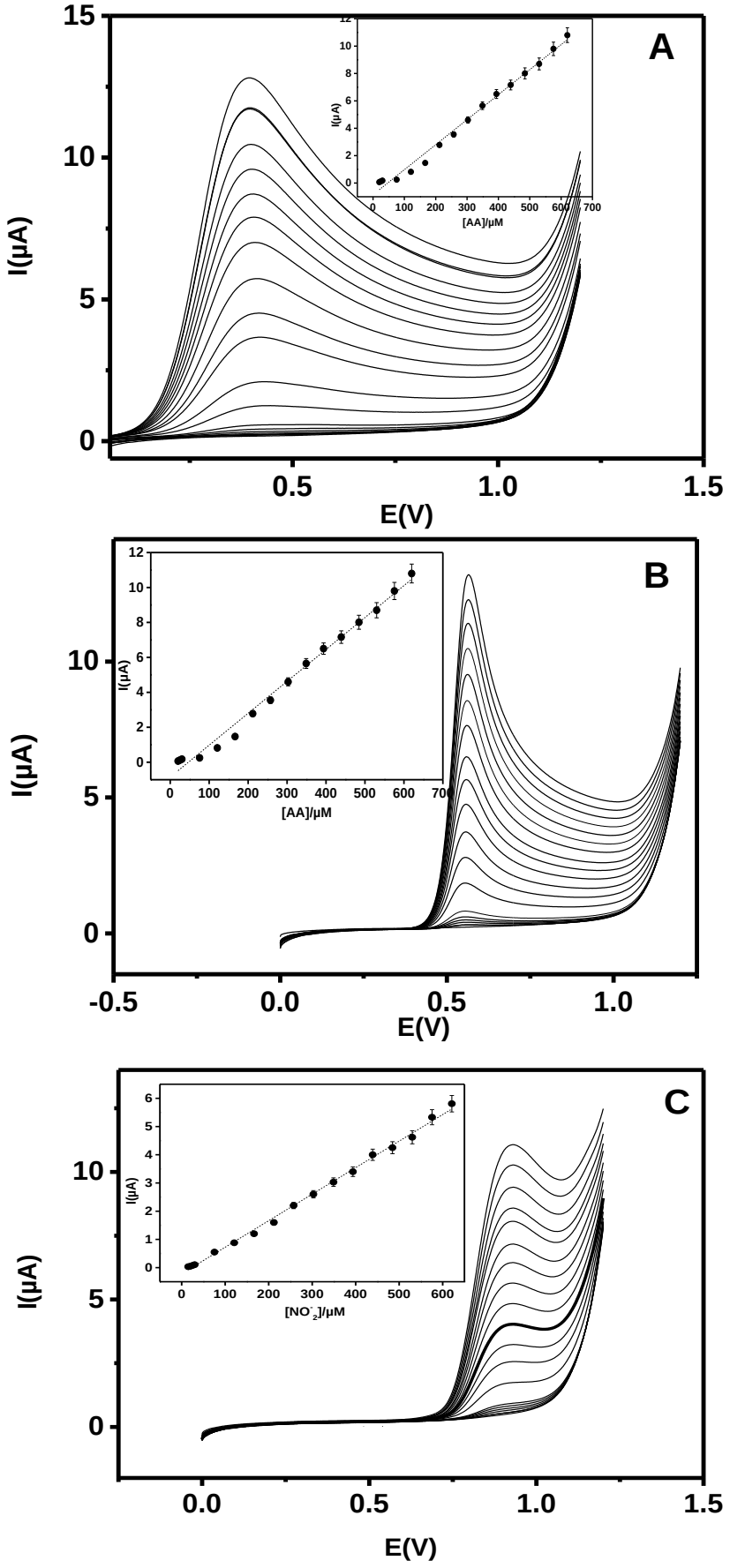

Fig. 7: LSVs recorded in 0.01 M AB (pH 5.0) at Sa-HTDMA/UiO-66/GCE with successive addition of AA (A), AC (B) and NO_2^- (C). The insets show the corresponding calibration curve.

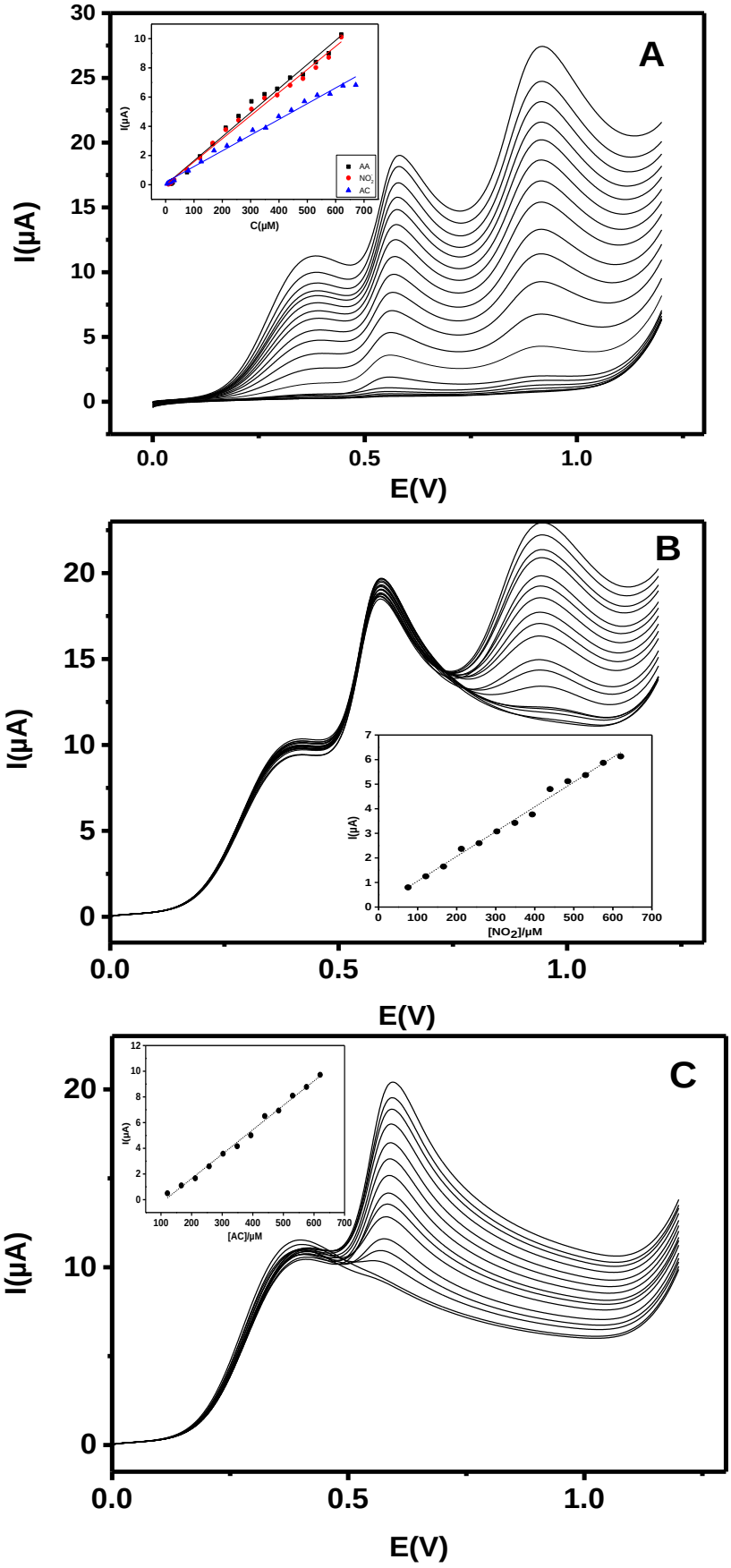
A
I(μA)
E(V)
C(μM)
AA
NO2
AC
B
I(μA)
E(V)
[NO2]/μM
C
I(μA)
E(V)
[AC]/μM

Fig. 8: LSVs recorded in 0.01 M AB (pH 5.0) at Sa-HTDMA/UiO-66/GCE with successive addition of (A) mixture of AA, AC and NO_2^-; (B) NO_2^- in the presence of fix concentration of AA and AC, and (C) AC in the presence of fix concentration of AA. The insets show the corresponding calibration curve.

Conclusion

An organoclay/UiO-66 composite film GCE was successfully fabricated by drop coating a suspension of the composite onto the electrode surface followed by drying at room temperature. The composite was obtained by mixing in a one-step procedure, an organoclay (Sa-HTDMA) (prepared by intercalating a cationic surfactant into the interlayer of the clay) with UiO-66. The fabricated Sa-HTDMA/UiO-66/GCE demonstrated high sensitivity and selectivity for the individual as well as concurrent detection of three analytes: AA, AC and NO_2^-, displaying low limits of detection and large concentration ranges. Although uric acid and dopamine were found to interfere with AA and AC, the electrochemical sensors prepared in this study were subsequently applied in the determination of AA and AC in pharmaceutical samples and nitrite in tap water. The developed strategy is promising for the routine determination of AA, AC and NO_2^- in real samples and quality control analysis owing to the facile fabrication of the sensor together with its high reproducibility and stability as well as the associated rapid analysis.

Experimental

Material, chemicals and reagents

The natural clay sample, namely "Sa", was sampled in a deposit on Sabga hill located in the West region of Cameroon in Central Africa. The clay consists predominantly of smectite with a trace amount of feldspar. The chemical composition and other characterisation of this clay have been reported [49]. Sa clay has a cation exchange capacity of 0.89 meq.g^{-1} and a BET surface area of 86 m^2 g^{-1}. The reagents and chemicals employed in this study were of analytical grade and were utilized as-received. Acetaminophen (95%), ascorbic acid (99%), dopamine (95%), uric acid (99%), caffeine (99%), hexadecyltrimethyl ammonium bromide (HDTMABr, 98%), $NaNO_2$ (99%), K_2HPO_4 (95%), KH_2PO_4 (99%), $K_3Fe(CN)_6$ (> 99%), KCl (99 %) and NaCl (99.5%) were from Abcr Chemicals. NaOH (97%), CH_3COOH (99%) and CH_3COONa (99%) were from STREM Chemicals. Zirconium tetrachloride (99.5 %), N,N dimethylformamide (DMF, 99.8%), terephthalic acid (98%), formic acid (95 %) were purchased from Sigma Aldrich.

Preparation of organoclay, Zr-MOF and organoclay/MOF composite

The sodium homoionic fine fraction of Sa clay (particle size less than 2 µm) was used to prepare organoclay. It was obtained by the sedimentation of pristine clay followed by conversion to its sodium form and then collected according to a previously reported procedure [21a]. Organoclay was prepared by stirring 1 g of the Sa homoionic fine fraction (denoted Sa-Na^+) at 250 rpm for 24 h in aqueous surfactant (HDTMABr) solution at 2.5 times the CEC so as to swell and to reach homogeneity. After centrifugation, the resulting organoclay, denoted Sa-HTMA, was recovered in solid form and then washed with water and ethanol to remove excess surfactant. The Sa-HTMA sample was dried in air for 48 h.

Zirconium-based MOF (UiO-66) was synthesized following the method reported by Ren et al [13] as follows: 0.22 mol of $ZrCl_4$ and 0.22 mol of terephthalic acid were added to DMF (50 mL) and then mixed thoroughly. Next, 100 mol equivalent of the modulator, formic acid, was added to the mixture. The mixture obtained was heated in an autoclave at 120 °C for 8 h. The product was left to cool to room temperature, followed by washing with DMF and drying under vacuum at 90 °C for 24 h. The obtained UiO-66 consisted of octahedral-shaped crystals of size 100-200 nm (from SEM images, Fig. 2A) with BET surface area of 1387 $m^2 g^{-1}$ and total pore volume of 0.51 $cm^3 g^{-1}$.

The clay-MOF composite was obtained by dispersing, in 2 mL of DMF, a given amount of the Zr-MOF (UiO-66) and the modified clay (Sa-HTMA). The mixture was kept under stirring for 48 h. The UiO-66 content was altered to 0, 20, 50, 60, 70 and 100 wt% by varying the amount of UiO-66 pre-dispersed solution.

Preparation of the working electrodes

Prior to use, glassy carbon electrode (GCE) employed as a substrate for the fabrication of the sensor was polished to a mirror-like surface on a wet cloth with 1, 0.3, and 0.05 µm aqueous alumina slurry. Then the electrode was rinsed with copious amounts of distilled water and cleaned sonically in 1:1 water/ethanol mixture for 30 minutes in order to eliminate any residual alumina. The films of Sa-HTDMA/UiO-66 were deposited onto the GCE surface by drop coating, whereby some microliters of colloidal Sa-HTDMA/UiO-66 composite dispersion in DMF was dropped onto the GCE. The coating was dried at room temperature for approximately 2 h. It was then rinsed with distilled water before use. The modified GCE, denoted Sa-HTDMA/UiO-66/GCE, was stored in acetate buffer (pH 5) when not in use. For the electrochemical characterization of Sa-HTDMA/UiO-66/GCE toward the anionic redox

probe ($Fe(CN)_6^{3-}$) in aqueous solution, 7 µL of Sa-HTDMA/UiO-66, UiO-66 and Sa-HTDMA suspensions were deposited on bare GCE by drop coating.

Instrumentation

Cyclic voltammetry (CV) and linear sweep voltammetry (LSV) experiments were performed using a ADLS DY 2323 Bi-potentiostat linked to the ALS2325EN electrochemical analysis system. All measurements were carried out in a conventional three electrodes cell assembly that is composed of $Ag/AgCl_{(KClsat)}$ reference electrode, a platinum wire counter electrode and a working electrode consisting of the modified glassy carbon. The identification of functional groups using FT-IR spectra was performed on an Alpha IR spectrometer (Bruker). IR spectra for all samples were recorded in the region 400-4500 cm^{-1}. X-ray diffraction (XRD) patterns of oriented films of pristine clay, UiO-66 and Sa-HTDMA/UiO-66 were recorded with 2θ scan step size of 0.026° using a PAN analytical X-Pert Pro X-ray powder diffractometer using Cu-Kα radiation (λ=1.54). The morphology of the MOF and composite materials was examined using a Zeiss Ultra PLUS FEG scanning electron microscope (SEM).

Supporting information summary

Additional figures (cyclic voltammograms, linear sweep voltammograms, plots of Ep versus log *v* and plot of Ep versus log I) and tables (determination of NO_2^- levels in tap water) are available in the supporting information.

CONFLICT OF INTEREST

There are no conflicts of interest to declare

Acknowledgement

The financial support from the Royal Society and UK aid (ROYAL SOCIETY –FCDO Grant AQ150029-ACBI programme) is gratefully acknowledged.

Keywords: Composite; Electroanalysis; Modified electrode; Organoclay; Zr-MOF

References

[1] E. L. Beard, *JONA's Healthc. Law Eth. Regul.* **2001**, *3*, 78-79.
[2] H. Beitollahi, A. Mohadesi, M. Mostafavi, H. Karimi-Maleh, M. Baghayeri and A. Akbari, *Ionics* **2014**, *20*, 729-737.
[3] F. Patel, *Medicine, Science and the Law* **1992**, *32*, 303-310.
[4] M. I. H. Helaleh and T. Korenaga, *Microchemical Journal* **2000**, *64*, 241-246.
[5] C. L. Walters, *Oncology* **1980**, *37*, 289-296.
[6] M. Grau, U. B. Hendgen-Cotta, P. Brouzos, C. Drexhage, T. Rassaf, T. Lauer, A. Dejam, M. Kelm and P. Kleinbongard, *Journal of Chromatography B* **2007**, *851*, 106-123.
[7] a) H. H. Awad and D. M. Stanbury, *International Journal of Chemical Kinetics* **1993**, *25*, 375-381; b) A. Wennmalm, G. Benthin, A. Edlund, L. Jungersten, N. Kieler-Jensen, S. Lundin, U. N. Westfelt, A. S. Petersson and F. Waagstein, *Circulation Research* **1993**, *73*, 1121-1127.
[8] Y.-G. Huang, J.-D. Ji and Q.-N. Hou, *Mutation Research/Fundamental and Molecular Mechanisms of Mutagenesis* **1996**, *358*, 7-14.
[9] A. Alonso, B. Etxaniz and M. D. Martinez, *Food Additives & Contaminants* **1992**, *9*, 111-117.
[10] Y. Zhang, L. Luo, Y. Ding and L. Li, *Microchimica Acta* **2009**, *167*, 123.
[11] B. O. Agboola, K. I. Ozoemena and T. Nyokong, *Electrochimica Acta* **2006**, *51*, 6470-6478.
[12] J.-M. Zen, A. S. Kumar and H.-W. Chen, *Electroanalysis* **2001**, *13*, 1171-1178.
[13] J. Ren, H. W. Langmi, B. C. North, M. Mathe and D. Bessarabov, *International Journal of Hydrogen Energy* **2014**, *39*, 890-895.
[14] V. Pascanu, G. González Miera, A. K. Inge and B. Martín-Matute, *Journal of the American Chemical Society* **2019**, *141*, 7223-7234.
[15] H.-Y. Li, S.-N. Zhao, S.-Q. Zang and J. Li, *Chemical Society Reviews* **2020**, *49*, 6364-6401.
[16] Y. Wang, H. Ge, G. Ye, H. Chen and X. Hu, *Journal of Materials Chemistry B* **2015**, *3*, 3747-3753.
[17] J. Zhou, X. Li, L. Yang, S. Yan, M. Wang, D. Cheng, Q. Chen, Y. Dong, P. Liu, W. Cai and C. Zhang, *Analytica Chimica Acta* **2015**, *899*, 57-65.
[18] Q. Wang, C. Gu, Y. Fu, L. Liu and Y. Xie, *Molecules* **2020**, *25*, 4557.
[19] J. C. Kemmegne-Mbouguen, F. P. Tchoumi, E. Mouafo-Tchinda, H. W. Langmi, S. E. Bambalaza, N. M. Musyoka, C. Kowenje and R. Mokaya, *New Journal of Chemistry* **2020**, *44*, 13108-13117.
[20] a) M. Massaro, G. Cavallaro, G. Lazzara and S. Riela in *13 - Covalently modified nanoclays: synthesis, properties and applications*, Eds.: G. Cavallaro, R. Fakhrullin and P. Pasbakhsh), Elsevier, **2020**, pp. 305-333; b) H. Zhu, J. Njuguna and M. A. Irfan in *9 - Clay minerals and solutions for green environment and human health*, Eds.: J. Njuguna, K. Pielichowski and H. Zhu), Woodhead Publishing, **2021**, pp. 211-223.
[21] a) J. C. Kemmegne-Mbouguen, I. T. Kenfack, A. Walcarius and E. Ngameni, *Talanta* **2011**, *85*, 754-762; b) J. C. Kemmegne-Mbouguen, H. E. Toma, K. Araki, V. R. L. Constantino, E. Ngameni and L. Angnes, *Microchimica Acta* **2016**, *183*, 3243-3253.
[22] L. Zhu, S. Tian and Y. Shi, *Clays and Clay Minerals* **2005**, *53*, 123-136.
[23] P. K. Ghosh and A. J. Bard, *The Journal of Physical Chemistry* **1984**, *88*, 5519-5526.
[24] a) J. C. Kemmegne-Mbouguen and E. Ngameni, *Analytical Methods* **2017**, *9*, 4157-4166; b) J. C. Kemmegne-Mbouguen, L. Angnes, E. Mouafo-Tchinda and E. Ngameni, *Electroanalysis* **2015**, *27*, 2387-2398.

[25] a) J. K. Mbouguen, E. Ngameni and A. Walcarius, *Biosens Bioelectron* **2007**, *23*, 269-275; b) J. Kemmegne Mbouguen, E. Ngameni and A. Walcarius, *Analytica Chimica Acta* **2006**, *578*, 145-155.
[26] J. C. Kemmegne-Mbouguen, E. Ngameni, P. G. Baker, T. T. Waryo2, B. Kgarebe and E. I. Iwuoha2, *Int. J. Electrochem. Sci.* **2014**, *9*, 478-492.
[27] a) H. He, R. L. Frost, T. Bostrom, P. Yuan, L. Duong, D. Yang, Y. Xi and J. T. Kloprogge, *Applied Clay Science* **2006**, *31*, 262-271; b) Z. Hu, G. He, Y. Liu, C. Dong, X. Wu and W. Zhao, *Applied Clay Science* **2013**, *75-76*, 134-140.
[28] M. Shirzad-Siboni, A. Khataee, A. Hassani and S. Karaca, *Comptes Rendus Chimie* **2015**, *18*, 204-214.
[29] J. H. Cavka, S. Jakobsen, U. Olsbye, N. Guillou, C. Lamberti, S. Bordiga and K. P. Lillerud, *J Am Chem Soc* **2008**, *130*, 13850-13851.
[30] a) M. S. Martin-González, M. A. García, I. Lorite, J. L. Costa-Krämer, F. Rubio-Marcos, N. Carmona and J. F. Fernández, *Journal of The Electrochemical Society* **2010**, *157*, E31; b) E. de Lucas-Gil, J. Menéndez, L. Pascual, J. F. Fernández and F. Rubio-Marcos, *Applied Sciences* **2020**, *10*, 1322.
[31] E. Ngameni, I. K. Tonlé, J. T. Apohkeng, R. G. B. Bouwé, A. T. Jieumboué and A. Walcarius, *Electroanalysis* **2006**, *18*, 2243-2250.
[32] C. Wang, R. Yuan, Y. Chai, S. Chen, Y. Zhang, F. Hu and M. Zhang, *Electrochimica Acta* **2012**, *62*, 109-115.
[33] P. D. James Speight, *Lange's Handbook of Chemistry, Sixteenth Edition*, McGraw-Hill Education, New York, **2005**, p.
[34] M. Arvand and T. M. Gholizadeh, *Colloids and Surfaces B: Biointerfaces* **2013**, *103*, 84-93.
[35] E. Laviron, *Journal of Electroanalytical Chemistry and Interfacial Electrochemistry* **1979**, *101*, 19-28.
[36] B. Ma, H. Guo, M. Wang, L. Li, X. Jia, H. Chen, R. Xue and W. Yang, *Electroanalysis* **2019**, *31*, 1002-1008.
[37] a) I. F. Hu and T. Kuwana, *Analytical Chemistry* **1986**, *58*, 3235-3239; b) H. Cheng, L. Li, M. Zhang, Y. Jiang, P. Yu, F. Ma and L. Mao, *TrAC Trends in Analytical Chemistry* **2018**, *109*, 247-259; c) P. Karabinas and D. Jannakoudakis, *Journal of Electroanalytical Chemistry and Interfacial Electrochemistry* **1984**, *160*, 159-167.
[38] M. H. Pournaghi-Azar and H. Dastangoo, *Journal of Electroanalytical Chemistry* **2004**, *567*, 211-218.
[39] Q. C. Meiling Liu, Cailang Lai, Youyu Zhang, Jianhui Deng, Haitao Li, Shouzhuo Yao, *Biosensors and Bioelectronics* **2013**, *48*, 75-81.
[40] N. H. Liuqing Yang, Qiujun Lu, Meiling Liu, Haitao Li, Youyu Zhang, Shouzhuo Yao, *Analytica Chimica Acta* **2015**.
[41] M. Saleh Mohammadnia, E. Marzi Khosrowshahi, E. Naghian, A. Homayoun Keihan, E. Sohouli, M. E. Plonska-Brzezinska, N. Ali Sobhani, M. Rahimi-Nasrabadi and F. Ahmadi, *Microchemical Journal* **2020**, *159*, 105470.
[42] K. Karaboduk, *ChemistrySelect* **2019**, *4*, 6361-6369.
[43] V. G. Dharmendra Kumar Yadav, Piyush Kumar Sonkar, Rupali Gupta, Pankaj Kumar Rastogi, *Electrochimica Acta* **2016**, *200*, 276-282.
[44] S. Duzmen, A. K. Baytak and M. Aslanoglu, *Materials Chemistry and Physics* **2020**, *252*, 123170.
[45] Y. R. Wang C1, Chai Y,Zhang Y,Hu F,Zhang M, *Biosensors and Bioelectronics* **2011**, *30*, 315-319.
[46] W. L. Yu Jun Yang, **2014**, *56* 300–306
[47] R. Yu Zhang, YaqinChai,WenjuanLi,XiaZhong,HuaanZhong, **2011**, *26*, 3977-3980.

[48] M. Shahbakhsh and M. Noroozifar, *Journal of Solid State Electrochemistry* **2018**, *22*, 3049-3057.
[49] I. K. Tonle, E. Ngameni, D. Njopwouo, C. Carteret and A. Walcarius, *Physical Chemistry Chemical Physics* **2003**, *5*, 4951-4961.

Table of content :

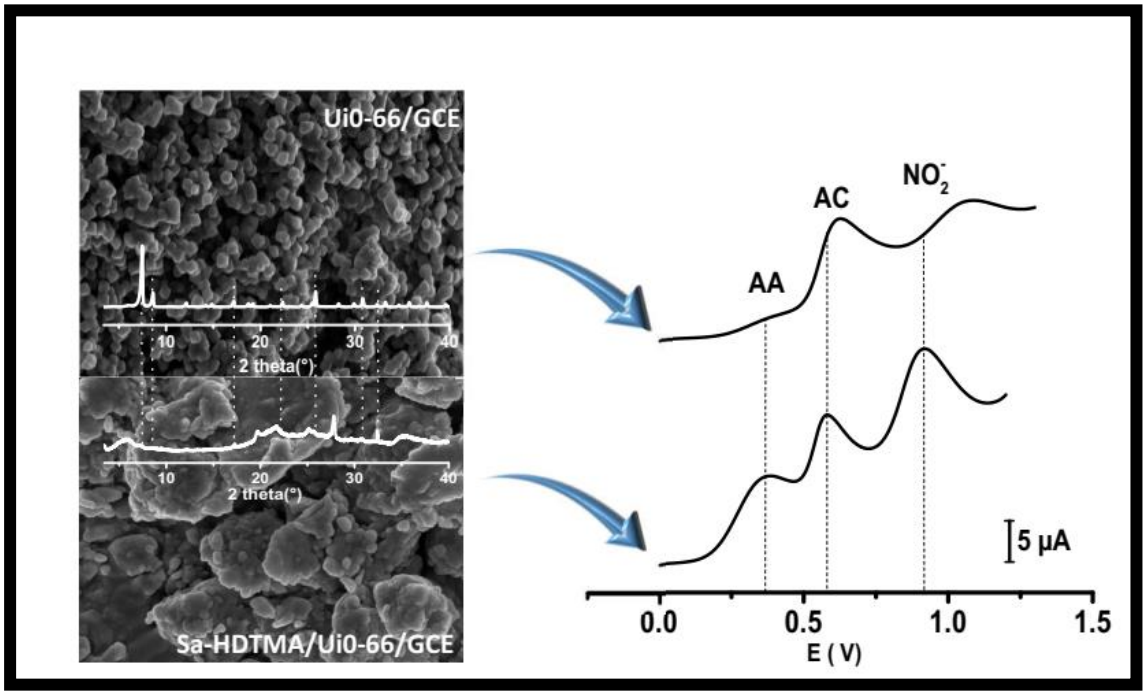

2- Highlight the novelty of the work

Taking advantage of the synergistic effect of clay and UiO-66 within a composite to form a stable film onto GCE for sensitive and selective electrochemical sensing